HHS Public Access

Author manuscript

NMR Biomed. Author manuscript; available in PMC 2017 October 01.

Published in final edited form as:

NMR Biomed. 2016 October ; 29(10): 1373–1380. doi:10.1002/nbm.3579.

Fast Volumetric Imaging of Bound and Pore Water in Cortical Bone Using Three-Dimensional Ultrashort Echo Time (UTE) and Inversion Recovery UTE (IR-UTE) Sequences

Jun Chen[1,2], **Michael Carl**[3], **Yajun Ma**[2], **Hongda Shao**[2], **Xing Lu**[2], **Bimin Chen**[2], **Eric Y Chang**[4,2], **Zhihong Wu**[1], and **Jiang Du**[2]

[1]Department of Orthopedics, Peking Union Medical College Hospital, Beijing, China

[2]Department of Radiology, University of California, San Diego, CA

[3]Applied Science Lab, GE Healthcare, San Diego, CA

[4]Radiology Service, VA San Diego Healthcare System, San Diego, CA

Abstract

We report the three-dimensional ultrashort echo time (UTE) and adiabatic inversion recovery UTE (IR-UTE) sequences employing a radial trajectory with conical view ordering for bi-component T_2^* analysis of bound water (T_2^{*BW}) and pore water (T_2^{*PW}) in cortical bone. An interleaved dual-echo 3D UTE acquisition scheme was developed for fast bi-component analysis of bound and pore water in cortical bone. A 3D IR-UTE acquisition scheme employing multiple spokes per IR was developed for bound water imaging. 2D UTE and IR-UTE sequences were employed for comparison. The sequences were applied to bovine bone samples (n=6) and volunteers (n=6) using a 3T scanner. Bi-component fitting of 3D UTE images of bovine samples shows a mean T_2^{*BW} of 0.26±0.04 ms and T_2^{*PW} of 4.16±0.35 ms, with fractions of 21.5±3.6% and 78.5±3.6%, respectively. The 3D IR-UTE signal shows a single-component decay with a mean T_2^{*BW} of 0.29±0.05 ms, suggesting selective imaging of bound water. Similar results were achieved with the 2D UTE and IR-UTE sequences. Bi-component fitting of 3D UTE images of the tibial midshafts of healthy volunteers shows a mean T_2^{*BW} of 0.32±0.08 ms and T_2^{*PW} of 5.78±1.24 ms, with a fraction of 34.2±7.4% and 65.8±7.4%, respectively. Single-component fitting of 3D IR-UTE images shows a mean T_2^{*BW} of 0.35±0.09 ms. The 3D UTE and 3D IR-UTE techniques allow fast volumetric mapping of bound and pore water in cortical bone.

Keywords

bone; UTE; IR-UTE; T_2^*; Cones; bound water; pore water

Corresponding Author: Jiang Du, Ph.D., jiangdu@ucsd.edu, University of California, San Diego, Department of Radiology, 200 West Arbor Drive, San Diego, CA 92103-8226, Phone (619) 471-0519, Fax (619) 471-0503.

Introduction

In normal cortical bone, the majority of water exists in the ‘bound’ form, either loosely bound to the organic matrix [1–3] or tightly bound to mineral [4–6], and a smaller fraction of water exists in the ‘free’ form, within the pores of the Haversian canals as well as in the lacunae and canaliculi systems [7–9]. The loosely bound water (BW) provides information on bone organic matrix density [1–3], while the pore water (PW) provides information on cortical porosity [9–12]. It is of central importance to separate these two water components as they provide complementary information about bone biomechanics [13].

A large number of studies suggest that bound and pore water in cortical bone samples can be reliably separated with multi-component T_2 analysis using high performance nuclear magnetic resonance (NMR) spectrometers [2, 8, 14]. However, this approach is not feasible on clinical whole-body MR scanners where radiofrequency (RF) power and gradient performance are reduced since the duration of the 180° pulse may be comparable or even longer than the T2s of bone water components, leading to an imperfect spin echo train for cortical bone. More recent studies suggest that bound and pore water in cortical bone can be imaged with ultrashort echo time (UTE) sequences using whole-body clinical magnetic resonance (MR) imaging scanners [15–19]. At 3T, bound water has a short T_2^* of ~ 0.3 ms and pore water has a T_2^* of ~ 2–5 ms, with both being detectable using UTE sequences with echo times (TEs) of less than 100 μs [7]. T_2^* of bound water is about 10 times shorter than that of pore water, and thus can be separated using UTE acquisitions with bi-component analysis [17]. Biswas et al. found that UTE bi-component analysis could reliably separate bound water from pore water, and reported a high correlation ($R^2 = 0.83$) between UTE measured pore water loss and gravimetric bone weight loss using sequential air-drying experiments [16]. Bae et al. reported a moderate correlation between pore water fraction and μCT porosity ($R^2 = 0.31$) and biomechanics ($R^2 = 0.22–0.30$) from a four-point bending test [15]. More recently, Seifert et al. reported a moderate correlation between short T_2^* fraction and μCT porosity ($R^2 = 0.70$ at 1.5T and 0.50 at 3T) as well as organic matrix density ($R^2 = 0.63$ at 1.5T and 0.44 at 3T) [9]. In another study, Rajapaske et al. found that both pore water fraction ($R^2 = 0.62$) and pore water T_2^* ($R^2 = 0.64$) were highly correlated with porosity index, a biomarker defined as the ratio of the UTE image intensities at a long and short TE [12].

Adiabatic inversion recovery UTE (IR-UTE) sequence has also been employed to selectively image bound water after pore water suppression [20–23]. Pore water has been shown to be effectively suppressed with a relatively broad range of inversion times (TIs) [21]. Fast pore water mapping can be achieved using a double adiabatic full passage (DAFP) sequence [20, 22, 23]. These novel sequences allow fast, volumetric mapping of bound and pore water in vivo.

In this study we report a new technique, referred to as 3D UTE imaging with a radial trajectory with conical view ordering [24,25], for fast bound and pore water imaging and separation through bi-component analysis [15–17]. The combination of adiabatic inversion recovery preparation pulse with the fast 3D UTE sequence (3D IR-UTE) was also proposed for volumetric imaging of bound water in vitro and in vivo. Studies involving bovine cortical

bone samples and tibial midshafts of healthy volunteers were performed to investigate the clinical feasibility of these novel techniques using a clinical whole-body 3T scanner.

Materials and Methods

Sample Preparation

Six bovine cortical bone samples were harvested from mature bovine femoral midshafts obtained from a local slaughterhouse, and were cleared of external muscle and soft tissue. Bone marrow was removed with a scalpel. Cross-sectional cortical bone segments with an approximate thickness of 80 mm were sectioned using a low-speed diamond saw (Isomet 1000, Buehler) with constant saline irrigation, and stored in phosphate buffered saline (PBS) solution for 24 hours prior to use.

Pulse Sequences

Figure 1 shows the 3D UTE sequence implemented on a 3T Signa TwinSpeed scanner (GE Healthcare Technologies, Milwaukee, WI). The basic 3D UTE sequence (Figure 1A) employs a short radio frequency (RF) rectangular pulse (duration = 26 μs) for signal excitation, followed by 3D radial trajectories with conical view ordering (Figure 1B) [25]. The 3D UTE sequence allows anisotropic resolution (e.g., high in-plane resolution and thicker slice) for much improved signal-to-noise ratio (SNR) and reduced scan time [26]. Eddy current artifacts are greatly reduced over the regular 2D UTE sequence, where half-pulse excitation creates sensitivity to eddy currents and gradient errors. A non-slice-selective 2D UTE sequence using a short rectangular pulse (duration = 26 μs) for signal excitation followed by 2D radial ramp sampling, was also employed for comparison [18]. The non-slice-selective 2D UTE sequence is insensitive to eddy currents and provides high SNR by integrating all signals along the slice dimension. It has been shown to provide reliable evaluation of bound and pore water in cortical bone [16, 18], and was used as a reference for the evaluation of the 3D UTE sequence.

Both bound water and pore water are detectable using the basic 3D UTE sequence with a minimum TE of 32 μs (Figure 1C). The 3D UTE sequence can also be combined with a relatively long adiabatic inversion recovery preparation pulse (Silver-Hoult pulse with duration of 8.64 ms) for 3D IR-UTE imaging of bound water (Figure 1D) [24]. The purpose of the long adiabatic IR pulse is to invert the longitudinal magnetization of the long T_2 signal components, including those in muscle and fat as well as pore water [7]. The longitudinal magnetization of bound water, which has a very short T_2^*, is not inverted but is largely saturated by the adiabatic IR pulse [20]. After an inversion time (TI) delay during which the inverted pore water magnetization approaches the null point, the Cones acquisition is initiated to selectively detect signal from bound water (Figure 1D). The adiabatic inversion preparation scheme was also combined with the non-slice-selective 2D UTE (2D IR-UTE) sequence and was used for comparison.

3D UTE T_2^* Analysis In Vitro

Each bovine cortical bone sample was placed in Fomblin solution (Ausimont, Thorofare, NJ), which helped maintain the hydration of cortical bone and minimize susceptibility

effects at tissue-air interfaces. A wrist coil (BC-10, Medspira, Minneapolis, MN) was used for signal excitation and reception. The imaging parameters for the basic single-echo 3D-UTE-Cones sequence are listed in Table 1. The acquired in-plane pixel size was 0.79×0.79 mm^2 with a sampling window of 624 μs and a total T_2^* quantification time of 37 min. The non-slice-selective 2D UTE sequence employed similar imaging parameters with 20 sec for each scan and the total T_2^* quantification time was 6 min. Detailed imaging parameters for the 2D non-slice-selective UTE sequence are also listed in Table 1.

To reduce the total scan time, we introduced an interleaved dual-echo 3D UTE data acquisition in which five sets of dual echo acquisitions (TEs = 0.03/2.2; 0.2/4.4; 0.4/6.6; 0.6/8.8; 0.8/11 ms) were acquired (referred to as the fast protocol). Other imaging parameters were similar to these used for single-echo 3D UTE data acquisition (referred as the slow protocol) as shown in Table 1. This interleaved dual-echo acquisition scheme reduced the total scan time from 37 min down to 11 min, which is acceptable for clinical scans and was used for in vivo studies (details follow).

The following bi-component analysis model was employed to analyze bound and pore water T_2^*s and their relative fractions [17, 27–29]:

$$SI(TE)=S_{0,BW}\times e^{-TE/T_2^{*BW}}+S_{0,PW}\times e^{-TE/T_2^{*PW}}+\text{Noise} \quad [1]$$

where $S_{0,BW}$ and $S_{0,PW}$ are the signal amplitude of bound and pore water components at TE of 0, and T_2^{*BW} and T_2^{*PW} are their T_2^* relaxation times. The fitting parameters are subject to the constraint of $S_{0,BW} + S_{0,PW} = 1$. Background noise was estimated using the widely used maximum likelihood estimation (MLE) distribution fitting algorithm [30–32]. As a result, only three parameters ($S_{0,BW}$ or $S_{0,PW}$, T_2^{*BW} and T_2^{*PW}) were fitted, greatly reducing the sensitivity to signal to noise ratio (SNR). In comparison, the following single-component analysis model was also employed to analyze the data [17, 27–29]:

$$SI(TE)=S_{0,}\times e^{-TE/T_2^*}+\text{Noise} \quad [2]$$

3D IR-UTE T_2^* Analysis In Vitro

Both 2D and 3D IR-UTE sequences have been proposed for selective imaging of bound water in cortical bone, with pore water being effectively suppressed by the adiabatic inversion pulse [18, 20–23]. In this study, we employed a similar idea but novel 3D radial trajectories with conical view ordering as well as anisotropic resolution to improve the acquisition efficiency. Moreover, we employed the acquisition of multiple radial trajectories (5 in this study) per adiabatic inversion pulse to further reduce the total scan time [24]. An odd number of spokes were employed (e.g., 3, 5, 7, etc.) with the middle spoke acquired at the null time (i.e., the inverted longitudinal magnetization of pore water reached the null point). The first half of the acquired spokes per IR preparation correspond to negative longitudinal magnetization of pore water, while the second half of the acquired spokes correspond to positive longitudinal magnetization of pore water. During re-gridding

reconstruction, the negative and positive magnetizations likely cancel, leading to excellent suppression of pore water. Several groups have employed this method (multiple spokes per IR preparation) to speed-up data acquisition while achieving efficient long T2 suppression [22, 23]. The imaging parameters for 2D non-slice-selective IR-UTE and 3D IR-UTE are listed in Table 1. Bi-component T_2^* analysis based on Eq.1 were performed on the 2D non-slice-selective IR-UTE and 3D IR-UTE images. Single-component fitting was also performed on the same data set for comparison.

3D UTE and IR-UTE T_2^* Analysis In Vivo

The 3D UTE and IR-UTE sequences were applied to the tibial midshafts of six healthy volunteers (all males, 28–44 years old, mean ± standard deviation = 34.6 ± 6.8). Written informed consent, approved by our Institutional Review Board, was obtained prior to their participation in this study. An 8-channel knee coil (Invivo Cooperation, Gainesville, Florida, USA) was used for signal excitation and reception. The fast 3D UTE and IR-UTE imaging protocol shown in Table 1 was used for in vivo studies. Both single-component and bi-component T_2^* analysis were performed on the 3D UTE and IR-UTE images.

Data Analysis

The analysis algorithm was written in Matlab (The MathWorks Inc., Natick, MA, USA) based on the Levenberg-Marquardt method for nonlinear least squares curve-fitting, and was executed offline on the DICOM images obtained by the protocols described above. The program allowed placement of ROIs on the first UTE image of the series, which was then copied onto each of the subsequent images. The mean intensity within each of the ROIs was used for subsequent curve fitting. The single- and bi-component exponential fitting models shown in Eq.2 and Eq.1 were used to fit the 2D UTE, 3D UTE, 2D IR-UTE and 3D IR-UTE images. Goodness of fit statistics, including the R-squared values and standard error or fitting confidence levels, were computed [17].

Results

Figure 2 shows selected 3D UTE and 3D IR-UTE images of a bovine cortical bone sample, as well as single- and bi-component fitting of the T_2^* decay curves from a representative ROI. Systematic residual signal is seen with single-component fitting of both single-echo and dual-echo 3D UTE images (results not shown), suggesting the existence of more than one water component. Excellent curve fitting was achieved with a bi-component model (Figures 2M and 2N). The bi-component fitting of single-echo 3D UTE images shows a short T_2^{*BW} of 0.26 ± 0.01 ms, accounting for 78.4% of the total bone signal decay, and a longer T_2^{*PW} of 4.08 ± 0.33 ms, accounting for 21.6% of the total signal decay. Very similar results were achieved with bi-component fitting of the single-echo 2D UTE and dual-echo 3D UTE images. Single-component and bi-component fitting of the 3D IR-UTE images shows exactly the same result, with a single T_2^* of 0.27 ms which is very close to the T_2^{*BW} of 0.26 ms. This further confirms that pore water with a longer T_2^* is inverted and nulled by the adiabatic IR pulse and bound water is selectively imaged with the 3D IR-UTE sequence.

Figure 3 shows bi-component analysis of 3D UTE images of a bovine cortical bone sample acquired with the slow single-echo protocol and fast dual-echo protocol, respectively. Compared to the slow single-echo protocol, the fast dual-echo 3D UTE imaging protocol provides 3.9% underestimation of T_2^{*BW} (0.25 vs. 0.26 ms), 3.5% overestimation of T_2^{*PW} (3.82 vs. 3.69 ms), near identical bound water fraction, and 2.4% overestimation of pore water fraction (25.4% vs. 24.8%). The comparable bound and pore water T_2^*s and relative fractions suggest that the dual-echo 3D UTE protocol can be used for fast volumetric mapping of bound and pore water, including their T_2^*s and relative fractions.

Figure 4 shows maps of bound and pore water T_2^*s and fractions derived from bi-component fitting of five sets of dual-echo 3D UTE images acquired in 9 min. Fairly homogenous bound water T_2^*s (~0.3 ms) and pore water T_2^*s (~4 ms) as well as bound water fractions (~80%) and pore water fractions (~20%) were demonstrated. The fast protocol employing five sets of dual-echo 3D UTE acquisitions shows similar maps as those derived from the slow protocol employing 17 sets of single-echo 2D UTE or 3D UTE (results not shown), except shorter pore water T_2^*s from the 2D UTE imaging.

Table 2 shows the mean and standard deviation of T_2^* values of six bovine bone samples. Bi-component fitting of 3D UTE images shows a mean pore water T_2^{*PW} of 4.24 ± 0.46 ms and bound water T_2^{*BW} of 0.26 ± 0.04 ms, with a fraction of 23.9 ± 3.4% and 76.1 ± 3.4%, respectively. These results are comparable to those derived from the 2D and 3D UTE single-echo acquisitions. The 3D IR-UTE signal shows an excellent single-component decay behavior, with a mean T_2^{*BW} of 0.29 ± 0.05 ms, which is slightly higher than the mean T_2^{*BW} of 0.27 ± 0.03 ms derived from single-component analysis of 2D IR-UTE images. Bi-component fitting of the 2D and 3D IR-UTE images shows near identical results as single-component fitting of the 2D and 3D IR-UTE images of bovine cortical bone samples.

Figure 5 shows representative 3D UTE and 3D IR-UTE images of the tibial midshaft of a 28-year-old volunteer. Cortical bone is barely visible using the 3D UTE sequence due to the high signal from surrounding long T_2 muscle and marrow fat. The 3D IR-UTE sequence efficiently suppressed signals from the surrounding long T_2 muscle and marrow fat, providing improved dynamic range and high signal from cortical bone. Excellent bi-component signal decay was observed with the 3D UTE images, with a short T_2^{*BW} of 0.36 ± 0.05 ms, accounting for 75.4% of the total bone signal decay, and a longer T_2^{*PW} of 5.56 ± 0.92 ms, accounting for 24.6% of the total signal decay. A single component was observed in the 3D IR-UTE images with a short T_2^{*BW} of 0.37 ± 0.04 ms. Maps of bound water and pore water T_2^*s as well as relative fractions were also displayed. About ~75% of bone water is bound to the organic matrix with T_2^*s of around 0.3–0.4 ms for this volunteer.

The mean and standard deviation of T_2^* values of the tibial midshafts of six healthy volunteers are also shown in Table 2. Bi-component fitting shows a mean pore water T_2^{*PW} of 5.78 ± 1.24 ms and bound water T_2^{*BW} of 0.34 ± 0.08 ms, with a fraction of 31.2 ± 6.1% and 68.8 ± 6.1%, respectively. Single-component fitting of 3D IR-UTE images shows a mean T_2^{*BW} of 0.37 ± 0.09 ms. Bi-component fitting of the 3D IR-UTE images shows near identical results as single-component fitting of the 3D IR-UTE images human tibial midshafts.

Discussion

Our data indicate that the fast 3D UTE sequence employing a radial trajectory with conical view ordering detects both bound water and pore water in cortical bone using a clinical whole-body 3T scanner. The excellent bi-component fitting suggests that two components are needed to explain the 3D UTE signal decay behavior. The majority of bone water (60–80%) exists in the form of bound water in cortical bone. The 3D IR-UTE signal decay shows excellent single-component decay behavior with a T_2^* similar to that of the shorter T_2^* component in bi-component analysis, suggesting that only bound water is detected. Our results confirm that pore water is likely being inverted and nulled by the adiabatic inversion preparation pulse and these findings are consistent with results reported in recent publications based on 2D UTE or IR-UTE sequences [7, 9–12], as well as earlier results based on multi-component analysis of FID data from NMR spectrometers [2, 8, 13, 14]. The 3D UTE and IR-UTE sequences allow for fast, volumetric assessment of bound and pore water in cortical bone in vivo, and may potentially be important for diagnosing osteoporosis and monitoring drug therapy.

The 3D UTE results from this study are largely consistent with those in the literature. Past NMR spectroscopy studies have confirmed the existence of multiple water components in cortical bone, with 70–90% water loosely bound to the organic matrix with a short T_2^* of ~0.3 ms, and 10–30% water residing in the pores with a longer T_2^* of 1–4 ms [2, 8, 13, 14]. Bi-component analysis of 3D UTE data shows a mean pore water T_2^* of 2.31 ± 0.34 ms for bovine cortical bone samples, and 1.97 ± 0.69 ms for tibial midshafts in vivo, and both are consistent with previously published values [2,8,13,14]. The bound water T_2^*s of 0.28 ± 0.01 ms for bovine cortical bone and 0.40 ± 0.09 for tibial midshafts in vivo are also consistent with values reported in the literature [2,8,13,14]. The bound and pore water fractions from bi-component analysis of 3D UTE images and 2D non-slice-selective UTE images are nearly identical, suggesting that the 3D UTE and 3D IR-UTE sequences can be readily used for clinical imaging purposes.

Similar to 2D UTE sequences, the 3D UTE sequence cannot detect water tightly bound to mineral and the collagen backbone protons. This pool of water demonstrates extremely short T_2^*s (< 10 μs) and is beyond the threshold to be directly detected using clinical whole-body scanners. However, signal from these protons may be indirectly detected using UTE combined with a magnetization preparation (MT) approach. A recent study suggests that UTE MT ratio (MTR) is moderately correlated with cortical porosity [33]. However, the correlation between UTE MTR and bone mineral content and bone matrix content remains to be investigated. The 3D UTE MT sequence may provide an approach for fast assessment of mineral bound water and collagen backbone protons using clinical MR scanners.

Bound and pore water mapping are of interest since they may allow for direct comparison between different groups of patients, including those with osteoporosis, renal osteodystrophy, Paget disease, and osteomalacia. The fast 3D UTE and IR-UTE sequences allow for volumetric mapping of bound and pore water T_2^*s and relative fractions. However, accurate bone water mapping requires T_1 and T_2/T_2^* correction since bound and pore water have not only different T_2^*s, but different T_1s [34]. The T_2^*s of bound and pore water can be

efficiently mapped with the 3D UTE bi-component analysis technique, but the T_1s of bound and pore water remain to be investigated. Bi-component fitting of saturation recovery UTE imaging is one approach [9], but can be time-consuming. Sequences with slightly longer TEs can potentially selectively detect signal from pore water, which has a longer T_2^*. Using the slightly longer TE, the signal from bound water is expected to be reduced to near zero, and can thus be used to measure T_1 of pore water [35]. IR-UTE sequences allow for selective imaging of bound water with pore water being inverted and nulled by the adiabatic inversion preparation pulse. IR-UTE sequences with different TR and TI combinations can be used to measure T_1 of bound water [36]. The use of the fast 3D UTE and IR-UTE sequences to measure T_1s of bound and pore water will be investigated in future studies, aiming to accurately map bound and pore water with T_1 and T_2^* compensation.

The interleaved dual-echo 3D UTE and IR-UTE acquisition techniques allow fast volumetric mapping of bound and pore water in cortical bone in vivo. Although they are more time-consuming than the 2D UTE and IR-UTE techniques, the 3D nature makes them suitable for bone water mapping not only in the tibial and femoral midshafts, but in locations where cortical bone is very thin, such as the femoral neck and distal radius regions. However, there are several limitations of this study. First, we demonstrate that two water components with distinct T_2^* values exist in cortical bone and can be separated with interleaved dual echo 3D UTE acquisitions. However, the accuracy of bound and pore water assessment, including T_2^* values and relative fractions remain to be investigated. Sequential air-drying and oven-drying studies together with gravimetrical analysis of bone samples may be useful. Second, the 3D IR-UTE sequence has shown potential in selective imaging of bound water with pore water being inverted and nulled by the adiabatic inversion preparation pulse. The multi-spoke acquisition per adiabatic IR preparation significantly reduces the total scan time, thus greatly facilitating potential clinical applications. However, when more spokes are being sampled per adiabatic IR preparation, significant pore water contamination may be introduced, and this requires further investigation. Third, the choice of TEs was empirical. The image signal is dominated by bone marrow and muscle in in-vivo imaging of cortical bone. In-phase imaging might have significantly higher signal than out-of-phase imaging, generating stronger streak artifacts. To keep a relatively constant imaging artifact level, we have chosen in-phase imaging for later echoes. Fourth, the 3D UTE bi-component analysis and 3D IR-UTE single-component analysis allows for fast, volumetric mapping of bound and pore water T_2^*s and relative fractions in vitro and in vivo. However, the clinical values of these techniques remain to be investigated.

In conclusion, we have demonstrated that bound and pore water in cortical bone can be reliably accessed with the fast 3D UTE and IR-UTE sequences using a clinical whole-body scanner. The T_2^*s of bound and pore water components can be reliably measured with the fast 3D UTE sequences presented in this study. Further clinical studies will be necessary to evaluate the diagnostic power of these methods, including studies involving patients with osteoporosis, osteomalacia, Paget disease, insufficiency fractures in the setting of biophosphonate therapy, and after raloxifene treatment.

Acknowledgments

The authors acknowledge grant support from GE Healthcare, NIH (1R01 AR062581-01A1, 1 R01 AR068987-01 and 1R21 AR063894-01A1), the VA Clinical Science Research and Development Service (Career Development Grant 1IK2CX000749), and the 'The International Postdoctoral Exchange Fellowship Program (No. 20130021)' from China.

Abbreviations used

2D	two-dimensional
3D	three-dimensional
3D UTE	three-dimensional ultrashort echo time imaging
3D IR-UTE	three-dimensional adiabatic inversion recovery ultrashort echo time imaging
AIR	adiabatic inversion recovery
BW	bound water
DAFT	double adiabatic full passage
FID	free induction decay
FOV	field of view
IR	inversion recovery
IR-UTE	inversion recovery UTE
MLE	maximum likelihood estimation
MR	magnetic resonance
MRI	magnetic resonance imaging
MT	magnetization transfer
MTR	magnetization transfer ratio
NEX	number of excitations
NMR	nuclear magnetic resonance
PBS	phosphate buffered saline
PW	pore water
RF	radio frequency
ROI	region of interest
SNR	signal to noise ratio
TE	echo time

μCT	micro computed tomography
UCSD	University of California, San Diego
UTE	ultrashort echo time

References

1. Cao H, Ackerman JL, Hrovat MI, Graham L, Glimcher MJ, Wu Y. Quantitative bone matrix density measurement by water- and fat-suppressed proton projection MRI (WASPI) with polymer calibration phantoms. Magn Reson Med. 2008; 60:1433–1443. [PubMed: 19025909]
2. Qingwen N, Jeffry SN, Xiaodu W, Armondo De Los S, Daniel PN. Assessment of water distribution changes in human cortical bone by nuclear magnetic resonance. Measurement Science and Technology. 2007; 18:715.
3. Wu Y, Chesler DA, Glimcher MJ, Garrido L, Wang J, Jiang HJ, Ackerman JL. Multinuclear solid-state three-dimensional MRI of bone and synthetic calcium phosphates. Proc Natl Acad Sci U S A. 1999; 96:1574–1578. [PubMed: 9990066]
4. Ivanova TI, Frank-Kamenetskaya OV, Kol'tsov AB, Ugolkov VL. Crystal Structure of Calcium-Deficient Carbonated Hydroxyapatite. Thermal Decomposition. Journal of Solid State Chemistry. 2001; 160:340–349.
5. Wilson EE, Awonusi A, Morris MD, Kohn DH, Tecklenburg MM, Beck LW. Highly ordered interstitial water observed in bone by nuclear magnetic resonance. J Bone Miner Res. 2005; 20:625–634. [PubMed: 15765182]
6. Wilson EE, Awonusi A, Morris MD, Kohn DH, Tecklenburg MM, Beck LW. Three structural roles for water in bone observed by solid-state NMR. Biophys J. 2006; 90:3722–3731. [PubMed: 16500963]
7. Du J, Hermida JC, Diaz E, Corbeil J, Znamirowski R, D'Lima DD, Bydder GM. Assessment of cortical bone with clinical and ultrashort echo time sequences. Magn Reson Med. 2013; 70:697–704. [PubMed: 23001864]
8. Horch RA, Nyman JS, Gochberg DF, Dortch RD, Does MD. Characterization of 1H NMR signal in human cortical bone for magnetic resonance imaging. Magn Reson Med. 2010; 64:680–687. [PubMed: 20806375]
9. Seifert AC, Wehrli SL, Wehrli FW. Bi-component T2 * analysis of bound and pore bone water fractions fails at high field strengths. NMR Biomed. 2015; 28:861–872. [PubMed: 25981785]
10. Bae WC, Patil S, Biswas R, Li S, Chang EY, Statum S, D'Lima DD, Chung CB, Du J. Magnetic resonance imaging assessed cortical porosity is highly correlated with muCT porosity. Bone. 2014; 66:56–61. [PubMed: 24928498]
11. Li C, Seifert AC, Rad HS, Bhagat YA, Rajapakse CS, Sun W, Lam SC, Wehrli FW. Cortical bone water concentration: dependence of MR imaging measures on age and pore volume fraction. Radiology. 2014; 272:796–806. [PubMed: 24814179]
12. Rajapakse CS, Bashoor-Zadeh M, Li C, Sun W, Wright AC, Wehrli FW. Volumetric Cortical Bone Porosity Assessment with MR Imaging: Validation and Clinical Feasibility. Radiology. 2015; 276:526–535. [PubMed: 26203710]
13. Horch RA, Gochberg DF, Nyman JS, Does MD. Non-invasive predictors of human cortical bone mechanical properties: T(2)-discriminated H NMR compared with high resolution X-ray. PLoS One. 2011; 6:e16359. [PubMed: 21283693]
14. Nyman JS, Ni Q, Nicolella DP, Wang X. Measurements of mobile and bound water by nuclear magnetic resonance correlate with mechancial properties of bone. Bone. 2008; 42:193–199. [PubMed: 17964874]
15. Bae WC, Chen PC, Chung CB, Masuda K, D'Lima D, Du J. Quantitative ultrashort echo time (UTE) MRI of human cortical bone: correlation with porosity and biomechanical properties. J Bone Miner Res. 2012; 27:848–857. [PubMed: 22190232]

16. Biswas R, Bae W, Diaz E, Masuda K, Chung CB, Bydder GM, Du J. Ultrashort echo time (UTE) imaging with bi-component analysis: bound and free water evaluation of bovine cortical bone subject to sequential drying. Bone. 2012; 50:749–755. [PubMed: 22178540]
17. Diaz E, Chung CB, Bae WC, Statum S, Znamirowski R, Bydder GM, Du J. Ultrashort echo time spectroscopic imaging (UTESI): an efficient method for quantifying bound and free water. NMR Biomed. 2012; 25:161–168. [PubMed: 21766381]
18. Chen J, Grogan SP, Shao H, D'Lima D, Bydder GM, Wu Z, Du J. Evaluation of bound and pore water in cortical bone using ultrashort-TE MRI. NMR Biomed. 2015; 28:1754–1762. [PubMed: 26527298]
19. Du J, Carl M, Bydder M, Takahashi A, Chung CB, Bydder GM. Qualitative and quantitative ultrashort echo time (UTE) imaging of cortical bone. J Magn Reson. 2010; 207:304–311. [PubMed: 20980179]
20. Horch RA, Gochberg DF, Nyman JS, Does MD. Clinically compatible MRI strategies for discriminating bound and pore water in cortical bone. Magn Reson Med. 2012; 68:1774–1784. [PubMed: 22294340]
21. Li S, Ma L, Chang EY, Shao H, Chen J, Chung CB, Bydder GM, Du J. Effects of inversion time on inversion recovery prepared ultrashort echo time (IR-UTE) imaging of bound and pore water in cortical bone. NMR Biomed. 2015; 28:70–78. [PubMed: 25348196]
22. Manhard MK, Horch RA, Gochberg DF, Nyman JS, Does MD. In Vivo Quantitative MR Imaging of Bound and Pore Water in Cortical Bone. Radiology. 2015; 277:221–229. [PubMed: 26020434]
23. Manhard MK, Horch RA, Harkins KD, Gochberg DF, Nyman JS, Does MD. Validation of quantitative bound- and pore-water imaging in cortical bone. Magn Reson Med. 2014; 71:2166–2171. [PubMed: 23878027]
24. Carl M, Bydder GM, Du J. UTE imaging with simultaneous water and fat signal suppression using a time-efficient multispoke inversion recovery pulse sequence. Magn Reson Med. 2015
25. Gurney PT, Hargreaves BA, Nishimura DG. Design and analysis of a practical 3D cones trajectory. Magn Reson Med. 2006; 55:575–82. [PubMed: 16450366]
26. Larson PE, Gurney PT, Nishimura DG. Anisotropic field-of-views in radial imaging. IEEE Trans on Med Imaging. 2008; 27:47–57.
27. Raya JG, Dietrich O, Horng A, Weber J, Reiser MF, Glaser C. T_2 measurement in articular cartilage: impact of the fitting method on accuracy and precision at low SNR. Magn Reson Med. 2010; 63:181–193. [PubMed: 19859960]
28. Reiter DA, Lin PC, Fishbein KW, Spencer RG. Multicomponent T2 relaxation analysis in cartilage. Magn Reson Med. 2009; 61:803–809. [PubMed: 19189393]
29. Anastasiou A, Hall LD. Optimization of T_2 and M_0 measurements of bi-exponential systems. Magn Reson Imaging. 2004; 22:67–80. [PubMed: 14972396]
30. Sijbers J, den Dekker AJ. Maximum Likelihood estimation of signal amplitude and noise variance from MR data. Magn Reson Med. 2004; 51:586–594. [PubMed: 15004801]
31. Dietrich O, Raya JG, Reiser MF. Magnetic resonance noise measurements and signal- quantization effects at very low noise levels. Magn Reson Med. 2008; 60:1477–1487. [PubMed: 19025912]
32. Aja-Fernandez S, Alberola-Lopez C, Westin CF. Noise and signal estimation in magnitude MRI and Rician distributed images: A LMMSE approach. IEEE Trans Image Proccess. 2008; 17:1383–1398.
33. Chang EY, Bae WC, Shao H, Biswas R, Li S, Chen J, Patil S, Healey R, D'Lima DD, Chung CB, Du J. Ultrashort echo time magnetization transfer (UTE-MT) imaging of cortical bone. NMR Biomed. 2015; 28:873–880. [PubMed: 25981914]
34. Techawiboonwong A, Song HK, Leonard MB, Wehrli FW. Cortical bone water: in vivo quantification with ultrashort echo-time MR imaging. Radiology. 2008; 248:824–833. [PubMed: 18632530]
35. Akbari A, Abbasi Rad S, Shojaie Moghadam M, Saligheh Rad H. T1 Quantification of the Cortical Bone Employing Short-TE MRI at 1.5 and 3 Tesla. Iran J Radiol. 2014; 11:e21303.
36. Du J, Sheth V, He Q, Carl M, Chen J, Corey-Bloom J, Bydder GM. Measurement of T1 of the ultrashort T2* components in white matter of the brain at 3T. PLoS One. 2014; 9:e103296. [PubMed: 25093859]

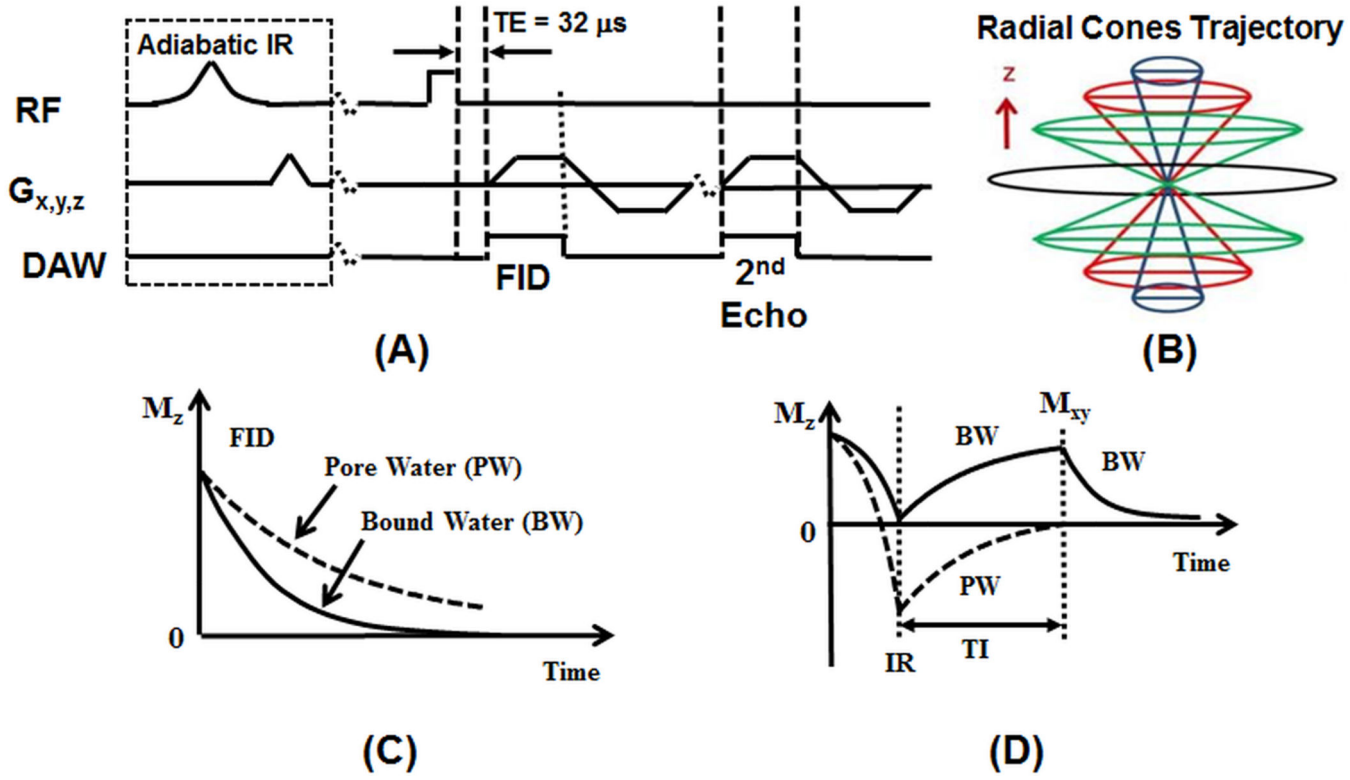

Figure 1.

The 3D UTE and IR-UTE sequences (A), and radial trajectories with conical view ordering in k-space (B), as well as the contrast mechanisms for UTE imaging of total water (B) and IR-UTE imaging of bound water (D). The 3D UTE sequence employs a short rectangular pulse for signal excitation followed by 3D radial ramp sampling with a minimal nominal TE of 32 μs, allowing detection of both bound and pore water (C). The 3D IR-UTE sequence employs an adiabatic inversion pulse to invert and null the pore water magnetization. The bound water magnetization is not inverted and is detected by a subsequent UTE data acquisition (D).

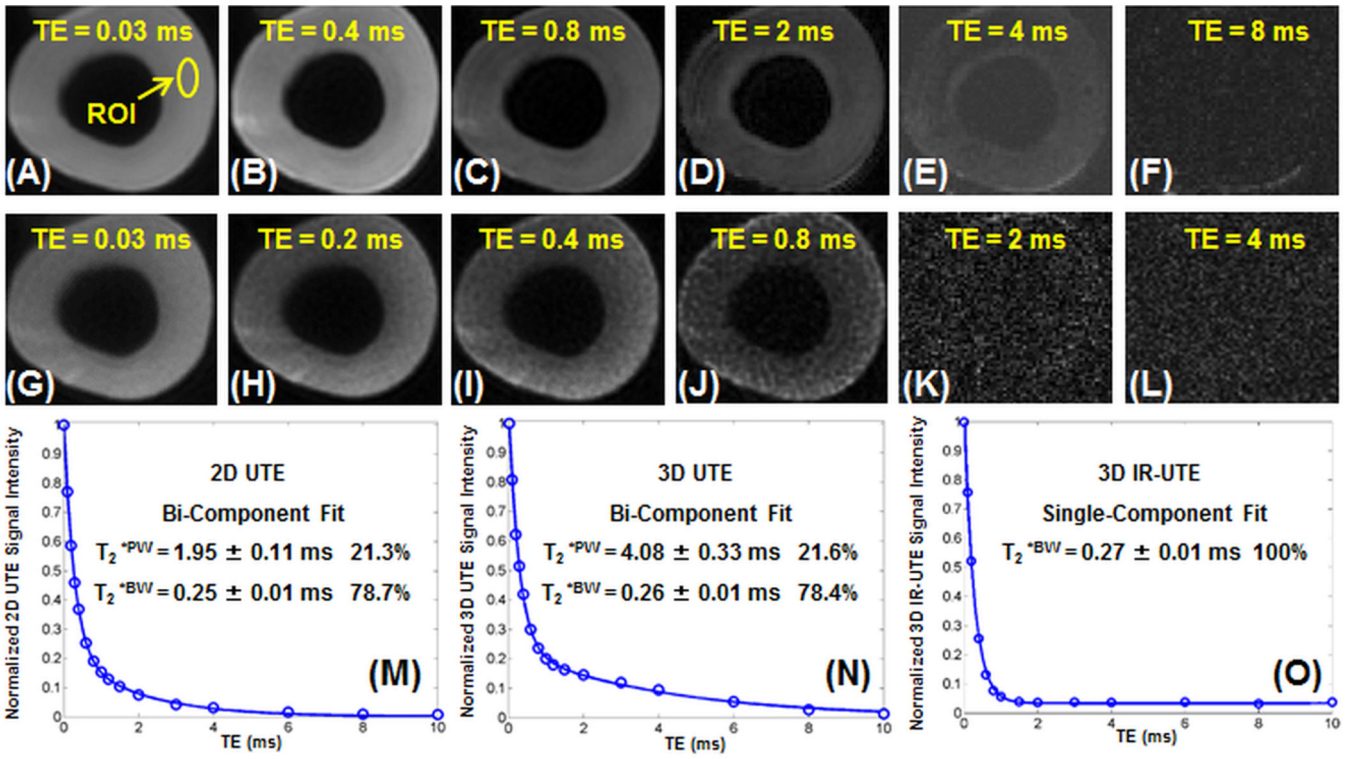

Figure 2.

Selected 3D-UTE-Cones imaging of a bovine cortical bone sample with TEs of 32 μs (A), 0.4 ms (B), 0.8 ms (C), 2 ms (D), 4 ms (E) and 8 ms (F), and 3D-UTE-IR-Cones imaging with TEs of 32 μs (G), 0.2 ms (H), 0.4 ms (I), 0.8 ms (J), 2 ms (K) and 4 ms (L), as well as bi-component fitting of signal from cortical bone acquired with 2D-UTE (M), 3D-UTE-Cones (N) and 3D-UTE-IR-Cones (O) images. Single-component fitting of the 2D-UTE and 3D-UTE-Cones images shows significant residual signal (results not shown). Excellent bi-component fitting is achieved for 2D-UTE and 3D-UTE-Cones images with similar T_2^*s and relative fractions as displayed in the fitting curves. A single-component decay is observed with the 2D-IR-UTE and 3D-UTE-IR-Cones images, consistent with pore water being nulled and bound water being selectively detected.

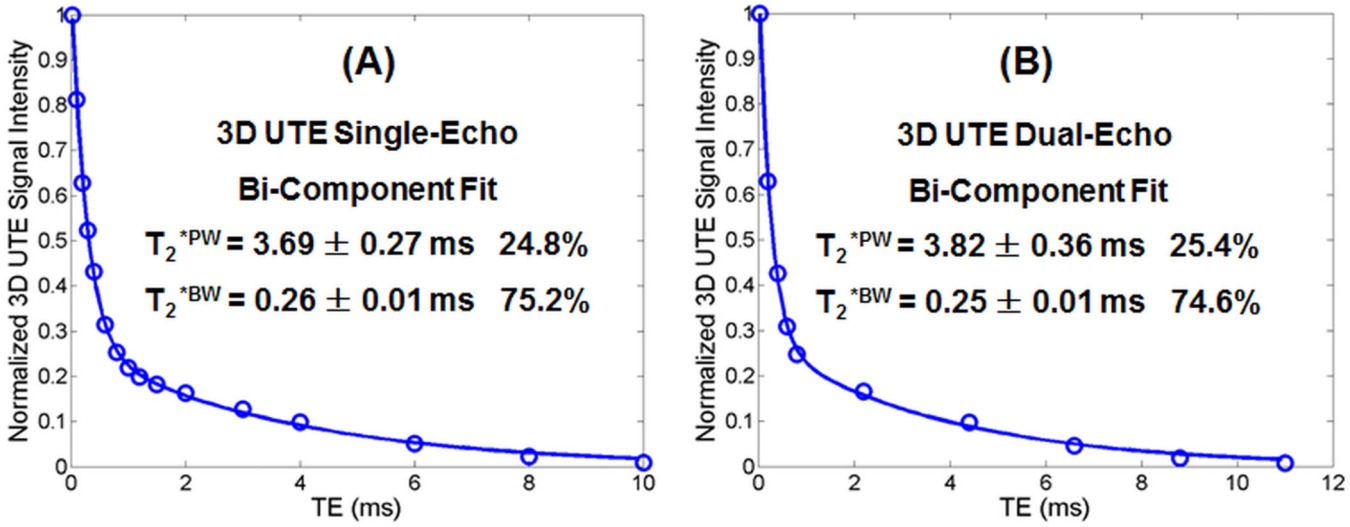

Figure 3.

Bi-component analysis of 3D UTE images of a bovine cortical bone sample acquired with the single-echo protocol (A) and dual-echo protocol (B). Bone images from the single-echo protocol show a bi-component T_2^* decay with a short T_2^{*BW} of 0.27 ± 0.01 ms and a longer T_2^{*PW} of 2.37 ± 0.36 ms, accounting for 73.4% and 26.6%, respectively. Bone images from the dual-echo protocol show a bi-component T_2^* decay with a short T_2^{*BW} of 0.27 ± 0.01 ms and a longer T_2^{*PW} of 2.26 ± 0.17 ms, accounting for 70.5% and 29.5%, respectively.

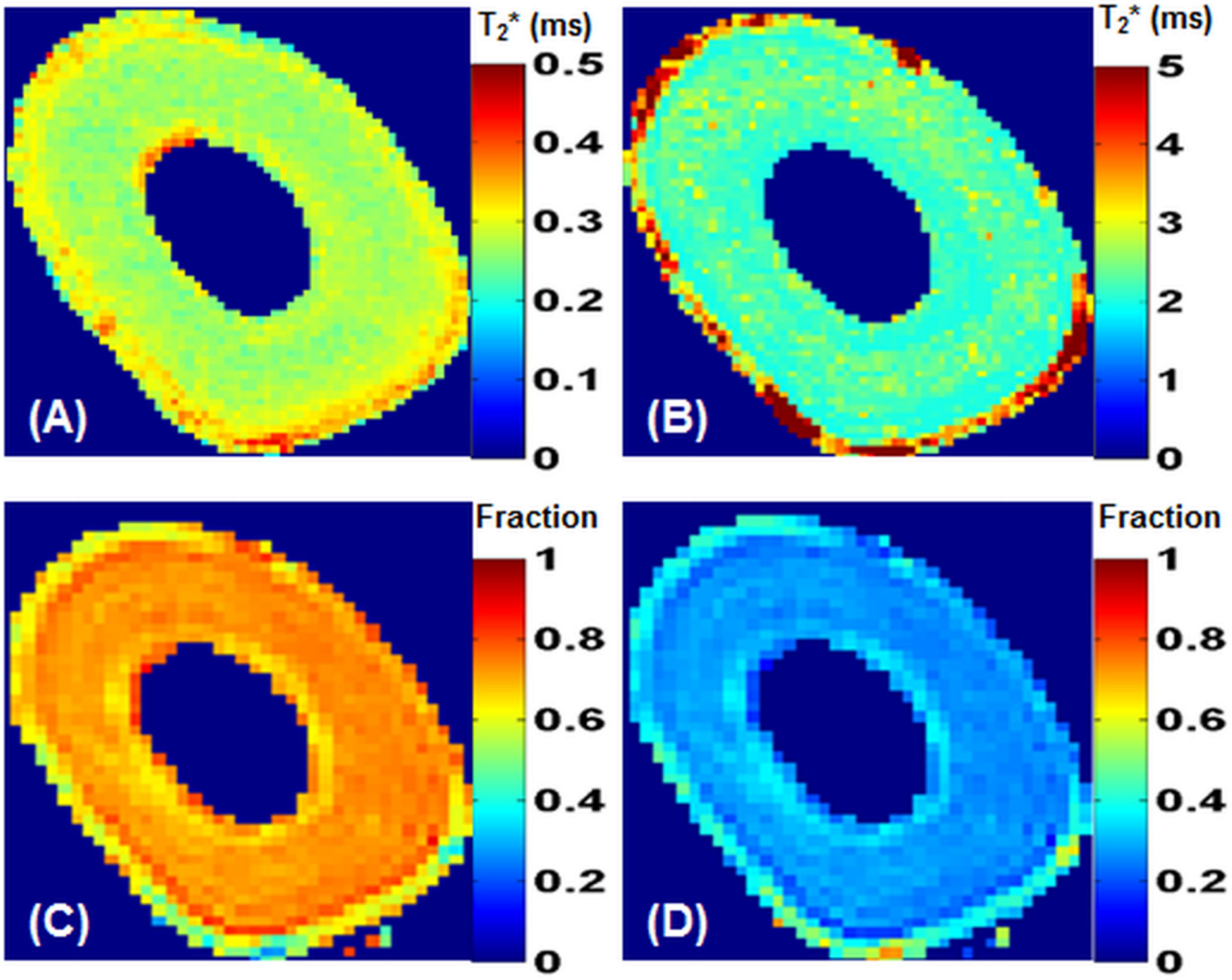

Figure 4.

Maps of bound water T_2^* (A), pore water T_2^* (B), bound water fraction (C) and pore water fraction (D) derived from bi-component fitting of five sets of dual-echo 3D-UTE-Cones images of a bovine cortical bone sample.

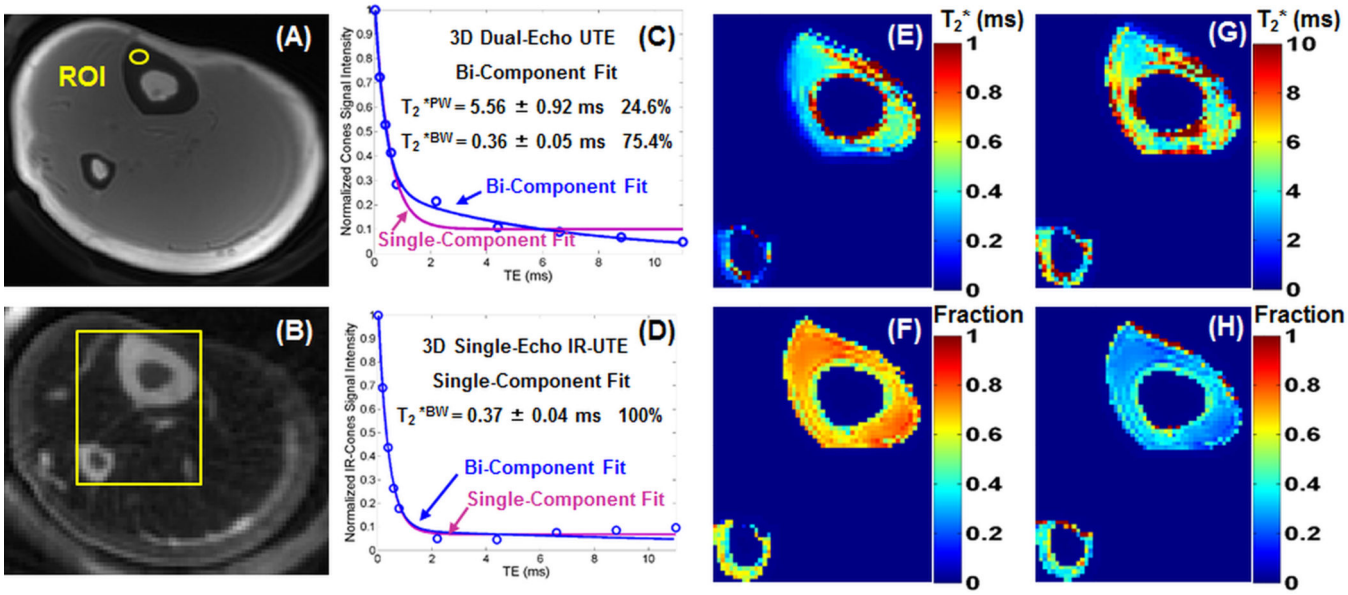

Figure 5.

Representative 3D–UTE-Cones (A) and 3D-UTE-IR-Cones (B) images of the tibial midshaft of a 28-year-old healthy volunteer, bi-component and single-component fitting of 3D-UTE-Cones images with a TE of 32 μs (C) and 3D-UTE-IR-Cones images with a TE of 32 μs (D), as well as maps of bound water T_2^* (E), bound water fraction (F), pore water T_2^* (G) and pore water fraction (H) derived from five sets of dual-echo bi-component fitting of 3D-UTE-Cones images in a total scan time of 9 min. The 3D-UTE-Cones images show a bi-component T_2^* decay with a short T_2^{*BW} of 0.36 ± 0.05 ms and a longer T_2^{*PW} of 5.56 ± 0.92 ms, accounting for 75.4% and 24.6%, respectively. A single component was observed in the 3D-IR-UTE-Cones images with a short T_2^{*BW} of 0.37 ± 0.04 ms.

Table 1

Imaging parameters for the slow protocol involving 2D UTE single-echo acquisition, 2D IR-UTE single-echo acquisition, 3D UTE single-echo acquisition and 3D IR-UTE single-echo acquisition, and the fast protocol involving 3D dual-echo UTE acquisition and 3D IR-UTE single-echo acquisition with reduced number of TEs (5 radial spokes were acquired per IR preparation in each 3D IR-UTE acquisition).

Sequences		TR (ms)	TE (ms)	TI (ms)	FOV (cm)	Acquisition Matrix	#spokes	#slice	Thickness (mm)	BW (kHz)	Flip Angle	Scan time (min)
Slow Protocol	2D UTE Single-Echo	100	0.008; 0.1; 0.2; 0.3; 0.4; 0.6; 0.8; 1; 1.2; 1.6; 2; 3; 4; 6; 8; 10	-	15	192 × 192	191	1	-	250	10°	0.32
	2D IR-UTE Single-Echo	100	0.008; 0.1; 0.2; 0.3; 0.4; 0.6; 0.8; 1; 1.2; 1.6; 2; 3; 4; 6; 8; 10	45	15	128 × 128	191	1	-	250	10°	0.32
	3D UTE Single-Echo	14.5	0.008; 0.1; 0.2; 0.3; 0.4; 0.6; 0.8; 1; 1.2; 1.6; 2; 3; 4; 6; 8; 10	-	15	192 × 192	7449	10	7	250	10°	1.8
	3D IR-UTE Single-Echo	100	0.03; 0.1; 0.2; 0.3; 0.4; 0.6; 0.8; 1; 1.2; 1.6; 2; 3; 4; 6; 8; 10	45	15	128 × 128	6131	10	7	250	10°	2.0
Fast Protocol	3D UTE Dual-Echo	14.5	0.03/2.2; 0.2/4.4; 0.4/6.6; 0.6/8.8; 0.8/11	-	15	192 × 192	7449	10	10	250	10°	1.8
	3D IR-UTE Single-Echo	100	0.03; 0.2; 0.4; 0.6; 0.8; 2.2; 4.4; 6.6; 8.8; 11.0	45	15	128 × 128	6131	10	10	250	10°	2.0

Table 2

Mean and standard deviation of T_2^{*PW}, T_2^{*BW}, PW fraction and BW fraction from bi-component fitting of 2D UTE, 3D UTE, 2D IR-UTE and 3D IR-UTE imaging of six bovine cortical bone samples, as well as six healthy volunteers.

Cortical Bone	T_2^* Measurements	T_2^{*PW}	T_2^{*BW}	T_2^{*PW} Fraction	T_2^{*BW} Fraction
Bovine Cortical Bone	2D UTE Single-Echo	2.12 ± 0.14 ms	0.25 ± 0.03 ms	20.6 ± 3.1%	79.4 ± 3.1%
Bovine Cortical Bone	2D IR-UTE Single-Echo	-	0.27 ± 0.03 ms	-	100%
Bovine Cortical Bone	3D UTE Single-Echo	4.16 ± 0.42 ms	0.26 ± 0.04 ms	21.5 ± 3.6%	78.5 ± 3.6%
Bovine Cortical Bone	3D UTE Dual-Echo	4.24 ± 0.46 ms	0.26 ± 0.04 ms	23.9 ± 3.4%	76.1 ± 3.4%
Bovine Cortical Bone	3D IR-UTE Single-Echo	-	0.29 ± 0.05 ms	-	100%
Volunteer Tibia Mid-shaft	3D UTE Dual-Echo	5.78 ± 1.24 ms	0.34 ± 0.08 ms	31.2 ± 6.1%	68.8 ± 6.1%
Volunteer Tibia Mid-shaft	3D IR-UTE Single-Echo	-	0.37 ± 0.09 ms	-	100%